# Safe Model-Free Optimal Voltage Control via Continuous-Time Zeroth-Order Methods

Xin Chen<sup>1</sup>, Jorge I. Poveda<sup>2</sup>, Na Li<sup>1</sup>

Abstract—To maintain voltage security with limited system model information, we develop a model-free optimal voltage control algorithm based on projected primal-dual gradient dynamics and continuous-time zeroth-order method (extremum seeking control). This proposed algorithm i) operates purely based on voltage measurements and does not require any other model information (model-free), ii) drives the voltage magnitudes back to the acceptable range while satisfying the power capacity constraints all the time (safety), and iii) minimizes the total operating cost (optimality). Moreover, this algorithm is implemented in a decentralized fashion where the privacy of controllable devices is preserved and plug-and-play operation is enabled. We prove that the proposed algorithm is semi-globally practically asymptotically stable and is structurally robust to small measurement noises. Lastly, the performance of this algorithm is further demonstrated via numerical simulations.

#### I. Introduction

Due to the rapidly increasing penetration of distributed energy resources (DERs), voltage control in distribution systems is confronted with new operational challenges, such as frequent over-voltage issues caused by reverse power flow, and growing uncertainty and volatility introduced by renewable generation. Many existing methods on voltage control [1], [2] are based on power flow models and assume good knowledge of distribution systems. In practice, high-accuracy network models and on-site identified parameters are unavailable for many distribution systems. Moreover, network reconfiguration, line faults, and other operational factors also change the system from time to time. Hence, it is desirable for voltage control to operate in the absence of system models and adapt fast to time-varying environments.

The deployment of smart meters and upgraded communication infrastructures offers an opportunity to overcome these challenges through real-time monitoring and control, which motivates the data-driven voltage control techniques. A type of such data-driven schemes [3]–[5] is to approximate the nonlinear power flow relation with a linear sensitivity model (e.g., the LinDistflow model [2]), and then to estimate the model online using measurement and regression methods. These schemes generally require a control center to store a large amount of metering data and solve high-dimensional regression problems in real-time. In contrast, *model-free control*, such as reinforcement learning (RL), does not explicitly

The work was supported by NSF CNS 1947613, NSF CAREER: ECCS-1553407 and NSF EAGER: ECCS-1839632.

estimate the system model but makes decisions directly based on measurements. A number of recent works [6], [7] propose to learn voltage control policies using various RL techniques. However, applying RL to the control of physical systems is still under development and has many limitations, such as safety issues, unstable training processes, limited or no theoretical guarantees, etc. See review article [8] and references therein for a more comprehensive view.

An alternative type of model-free control is based on zeroth-order (or gradient-free) methods [9]. In particular, extremum seeking (ES) control [10], [11] is a classic continuous-time zeroth-order method developed to solve real-time optimization problems, which operates by using only the output measurements. ES control attracts surging recent attention and has been applied in broad power system applications, including energy consumption control [12], voltage phasor regulation [13], maximum power point tracking [14], etc. Moreover, [15], [16] propose ES control algorithms to modulate the power injections of DERs for voltage regulation. In [17], hardware-in-the-loop experiments are conducted to verify the viability of a ES-based voltage control scheme. Despite these progresses, one major limitation of existing ES algorithms is that constraints are not well addressed. Most ES methods consider unconstrained optimization for simplicity or penalize the constraint violation in the objective. However, there are various physical constraints, e.g., the power capacity limits, that need to be enforced for safe operation.

Contributions. In this paper, we study the real-time voltage control through modulating the active and reactive power outputs of fast time-scale controllable devices. To overcome the challenges described above, we develop a model-free optimal voltage control algorithm based on projected primal-dual gradient dynamics (P-PDGD) and ES control. Specifically, by leveraging the structure of P-PDGD, the proposed algorithm can steer the system to an optimal operating point while satisfying the physical constraints. Then, ES control is adopted to make this algorithm "model-free" in the sense that the distribution system model is circumvented. The main merits of the proposed algorithm are explained as below:

- (*Safety and Optimality*). The proposed algorithm drives the voltage magnitudes back to the acceptable range while always satisfying the power capacity constraints, and minimizes the total operating cost.
- (*Model-Free*). The proposed algorithm is an end-to-end model-free control method that operates purely based on the voltage measurements from the monitored buses. The model information of distribution networks and

<sup>&</sup>lt;sup>1</sup>X. Chen and N. Li are with the School of Engineering and Applied Sciences, Harvard University, USA; chen\_xin@g.harvard.edu, nali@seas.harvard.edu. <sup>2</sup>J. I. Poveda is with the Department of Electrical, Computer, and Energy Engineering at the University of Colorado, Boulder, USA; jorge.poveda@colorado.edu.

- other power injections is not needed.
- (Adaptive). By exploiting real-time measurement, this
  algorithm is a feedback mechanism that can adapt fast
  to changes in the dynamical system environment.
- (Decentralized). This algorithm is implemented in a decentralized manner, where the privacy of each device can be preserved. Moreover, it allows plug-and-play operation and thus is robust to single/multi-point failures.
- (Guaranteed Performance). We mathematically prove the semi-global practical asymptotical stability and the structural robustness (to small measurement noise) of the proposed algorithm, and numerically verify its effectiveness, optimality and robustness via simulations.

To the best of our knowledge, this is the first work on voltage control that unifies all the above features. We also emphasize that the proposed ES-P-PDGD algorithm is a generic model-free method that can be applied to many other multi-agent optimization and control problems.

Lastly, we mention a closely-related work [18]. It proposes a model-free primal-dual projected gradient algorithm for real-time optimal power flow based on discrete-time zeroth-order methods, but it makes strong assumptions on the problem setting and lacks explicit convergence results. In contrast, this paper uses and studies the continuous-time ES control dynamics, and provides clear stability guarantee. Besides, distinguished from the projection method used in [18], our algorithm employs the global projection and it leads to a *Lipschitz continuous* projected dynamical system (see Remark 2), which facilitates the theoretical analysis.

**Notations.** We use unbolded lower-case letters for scalars, and bolded lower-case letters for column vectors.  $|\cdot|$  denotes the cardinality of a set.  $||\cdot||$  denotes the L2-norm of a vector.  $[x;y]:=[x^\top,y^\top]^\top$  denotes the column merge of vectors x,y.  $\mathbb{R}_+:=[0,+\infty)$  is the set of non-negative real values.

## II. OPTIMAL VOLTAGE CONTROL PROBLEM

Consider a distribution network with the monitored bus set  $\mathcal{M}$  and the controllable device set  $\mathcal{C}$ . Each bus  $j \in \mathcal{M}$  has real-time voltage measurement, and the power injection of each device  $i \in \mathcal{C}$  can be adjusted for voltage regulation. Depending on the practical system configuration, the controllable devices are flexible to locate at any buses of the distribution network. The optimal voltage control (OVC) problem is formulated as model (1) and explained below:

Obj. 
$$\min_{\boldsymbol{x}} \sum_{i \in \mathcal{C}} c_i(\boldsymbol{x}_i)$$
 (1a)

s.t. 
$$x_i \in \mathcal{X}_i$$
,  $i \in \mathcal{C}$  (1b)

$$\underline{v}_i \le v_j(\boldsymbol{x}) \le \bar{v}_j, \qquad j \in \mathcal{M}.$$
 (1c)

1) Decision Variable and Feasible Set: The decision variable  $x_i$  is the power injection of controllable device  $i \in \mathcal{C}$ , and its power capacity constraints are described with the feasible set  $\mathcal{X}_i$  in (1b). Define  $x := (x_i)_{i \in \mathcal{C}}$ ,  $\mathcal{X} := \prod_{i \in \mathcal{C}} \mathcal{X}_i$ . Specifically, we consider the following two types of devices for real-time voltage control with  $\mathcal{C} = \mathcal{C}_{\text{svc}} \cup \mathcal{C}_{\text{dg}}$ :

i) Static Var Compensator (SVC) with the reactive power injection  $x_i := q_i$  and the power capacity constraint (2):

$$\mathcal{X}_i := \{ \boldsymbol{x}_i | q_i \le q_i \le \bar{q}_i \}, \quad i \in \mathcal{C}_{\text{svc}}$$
 (2)

where  $\bar{q}_i$  and  $\underline{q}_i$  are the upper and lower limits, respectively. ii) Distributed Generation (DG) with the active and reactive power injection  $\boldsymbol{x}_i := [p_i, q_i]^{\top}$  and constraint (3):

$$\mathcal{X}_i := \{ \mathbf{x}_i | p_i \le p_i \le \bar{p}_i, p_i^2 + q_i^2 \le \bar{s}_i^2 \}, \quad i \in \mathcal{C}_{dg}$$
 (3)

where  $\bar{p}_i$  and  $\underline{p}_i$  are the upper and lower limits of active power, and  $\bar{s}_i$  denotes the apparent power capacity.

- 2) Network and Voltage Constraints:  $v_j$  in (1c) denotes the voltage magnitude at bus  $j \in \mathcal{M}$ , and  $\underline{v}_j$  and  $\bar{v}_j$  are the lower and upper voltage limits, respectively. We use the functional form  $v_j(\boldsymbol{x})$  to describe the input-output map from the controllable power injection  $\boldsymbol{x}$  to the voltage magnitude  $v_j$ . Essentially,  $\boldsymbol{v}(\boldsymbol{x}) := (v_j(\boldsymbol{x}))_{j \in \mathcal{M}}$  captures the nonconvex power flow equations, distribution network model, and other uncontrollable power injections; see [1], [5] for details.
- 3) Objective Function: The objective (1a) aims to minimize the total operating cost with the cost function  $c_i(\cdot)$  for each device  $i \in \mathcal{C}$ . For instance, the quadratic cost function  $c_i(x_i) = x_i^{\top} \Sigma_i x_i$  is a widely used objective [1], [5], where  $\Sigma_i$  is the diagonal matrix of cost coefficients.

We summarize the known and unknown information in our problem setting with the following assumption.

**Assumption 1.** The gradient of the individual cost function, i.e.,  $\nabla c_i(\cdot)$ , exists and is known to each device  $i \in \mathcal{C}$  itself, as well as the feasible set  $\mathcal{X}_i$ . The system model, i.e., function v(x), is unknown but the real-time voltage measurement of v is available.

**Remark 1.** In this work, we consider a general convex cost function  $c_i(\boldsymbol{x}_i)$ , while the quadratic cost function is only adopted for simulations. Besides, we assume that the gradient  $\nabla c_i(\boldsymbol{x}_i)$  is known to each device for simplicity. Nevertheless, the proposed voltage control algorithm is applicable to the case when  $\nabla c_i(\boldsymbol{x}_i)$  and  $c_i(\boldsymbol{x}_i)$  are unknown but the cost value  $c_i$  can be measured in real time. Similarly, if the real-time measurement of network loss is available, the cost of network loss  $\ell(\boldsymbol{x})$  can be also included in objective (1a).

## III. ALGORITHM DESIGN

In this paper, we aim to design a real-time voltage control algorithm that satisfies the following four requirements:

- 1) **Asymptotic voltage limits**. Once a disturbance occurs, the controller can drive the monitored voltage magnitudes  $(v_j)_{j \in \mathcal{M}}$  back to the acceptable interval  $[\underline{v}_j, \overline{v}_j]$ .
- 2) Hard capacity constraints. The power injection  $x_i$  of the controllable device  $i \in \mathcal{C}$  should satisfy the physical power capacity constraints  $\mathcal{X}_i$  at all times.
- 3) **Optimality**. The controllable devices should be regulated in an economically efficient way that minimizes the total operating cost.
- Model-free. Information of the power network (topology and line parameters), loads and other power injections is not required.

To this end, we firstly solve the OVC model (1) with the projected primal-dual gradient dynamics, so that the solution dynamics can be interpreted as the voltage controller which meets the first three requirements above. Then we take the fourth requirement into account and develop a model-free voltage control algorithm based on ES control.

#### A. Projected Primal-Dual Gradient Dynamics

We make the following two standard assumptions on the OVC model (1) to render it a convex optimization problem with strong duality. We emphasize that these assumptions are mainly for theoretical analysis, and the proposed control algorithm can be applied to power systems with a nonlinear power flow model, which is validated by our simulations.

**Assumption 2.** For all  $i \in \mathcal{C}$ , the function  $c_i(\cdot)$  is convex and has locally Lipschitz gradients, and the set  $\mathcal{X}_i$  is closed and convex. Also, the function  $v_j(\cdot)$  is affine for all  $j \in \mathcal{M}$ .

**Assumption 3.** The OVC problem (1) has a finite optimum, and the Slater's conditions hold for the problem (1).

We employ the projected primal-dual gradient dynamics (P-PDGD) method to solve the OVC model (1). With dual variables  $\lambda^+ := (\lambda_i^+)_{i \in \mathcal{M}}, \lambda^- := (\lambda_i^-)_{i \in \mathcal{M}}$ , the saddle point problem of the OVC model (1) is formulated as

$$\max_{\boldsymbol{\lambda} \geq 0} \min_{\boldsymbol{x} \in \mathcal{X}} L(\boldsymbol{x}, \boldsymbol{\lambda}) = \sum_{i \in \mathcal{C}} c_i(\boldsymbol{x}_i) + \sum_{j \in \mathcal{M}} \left[ \lambda_j^+(v_j(\boldsymbol{x}) - \bar{v}_j) + \lambda_j^-(\underline{v}_j - v_j(\boldsymbol{x})) \right],$$
(4)

where  $\lambda := [\lambda^+; \lambda^-]$  and  $L(x, \lambda)$  denotes the Lagrangian function. Then we solve problem (4) with P-PDGD (5):

$$\dot{\boldsymbol{x}}_{i} = k_{x} \left[ \operatorname{Proj}_{\mathcal{X}_{i}} \left( \boldsymbol{x}_{i} - \alpha_{x} \frac{\partial L(\boldsymbol{x}, \boldsymbol{\lambda})}{\partial \boldsymbol{x}_{i}} \right) - \boldsymbol{x}_{i} \right], \quad i \in \mathcal{C} \quad (5a)$$

$$\dot{\lambda}_{j}^{+} = k_{\lambda} \left[ \operatorname{Proj}_{\mathbb{R}_{+}} \left( \lambda_{j}^{+} + \alpha_{\lambda} (v_{j}(\boldsymbol{x}) - \bar{v}_{j}) \right) - \lambda_{j}^{+} \right], \quad j \in \mathcal{M} \quad (5b)$$

$$\dot{\lambda}_{j}^{-} = k_{\lambda} \left[ \operatorname{Proj}_{\mathbb{R}_{+}} \left( \lambda_{j}^{-} + \alpha_{\lambda} (\underline{v}_{j} - v_{j}(\boldsymbol{x})) \right) - \lambda_{j}^{-} \right], \quad j \in \mathcal{M} \quad (5c)$$

where  $k_x, k_\lambda, \alpha_x, \alpha_\lambda$  are positive parameters, the Lipschitz projection operator  $\operatorname{Proj}_{\mathcal{X}}(\cdot)$  is defined as  $\operatorname{Proj}_{\mathcal{X}}(x) :=$  $\operatorname{argmin} ||y - x||$ , and the gradient in (5a) is given by  $y \in \mathcal{X}$ 

$$\frac{\partial L(\boldsymbol{x}, \boldsymbol{\lambda})}{\partial \boldsymbol{x}_i} = \nabla c_i(\boldsymbol{x}_i) + \sum_{j \in \mathcal{M}} (\lambda_j^+ - \lambda_j^-) \frac{\partial v_j(\boldsymbol{x})}{\partial \boldsymbol{x}_i}.$$
 (6)

Denote  $z:=[x;\lambda]$  and define  $\mathcal{Z}:=\mathcal{X}\times\mathbb{R}^{2|\mathcal{M}|}_{\perp}$  as the feasible set of z in (5).

Remark 2. (Projection of Dynamical System) The projection method used in (5) is referred as global projection [19]. By [19, Lemma 3], it ensures that  $z(t) \in \mathcal{Z}$  for all time  $t \geq t_0$ when the initial condition  $z(t_0) \in \mathcal{Z}$ . Note that the P-PDGD (5) is Lipschitz continuous; it differs from other types of discontinuous projections considered in literature, e.g., [18], [20], [21], which project the dynamics onto the tangent cone of the feasible set, and thus they need the analytical tools for discontinuous dynamical systems.

The stability of the P-PDGD (5) is stated as Theorem 1.

Theorem 1. (Global Asymptotical Stability.) Under Assumption 2 and 3, with initial condition  $z(t_0) \in \mathcal{Z}$ , the trajectory z(t) of the P-PDGD (5) will stay within Z for all  $t \geq t_0$ , and globally asymptotically converge to an optimal solution  $z^* := [x^*; \lambda^*]$  of the saddle point problem (4), where  $x^*$  is an optimal solution of the OVC problem (1).

The proof of Theorem 1 mainly follows the asymptotical stability of globally projected (primal-dual) dynamical systems [22, Lemma 2.4] [19]. A detailed proof is provided in the online version of this paper [23].

## B. Model-Free Voltage Control Algorithm

The P-PDGD (5) cannot be implemented without knowledge of the system model v(x), since there are two occasions in the P-PDGD (5) where this model is needed:

- 1) The gradients  $\frac{\partial v_j(\boldsymbol{x})}{\partial \boldsymbol{x}_i}$  in (6) for  $i \in \mathcal{C}, j \in \mathcal{M}$ ; 2) The functions  $v_j(\boldsymbol{x})$  in (5b) (5c) for  $j \in \mathcal{M}$ .

To develop a model-free controller, accordingly, we propose two strategies. Strategy 1): use ES control to estimate the gradients  $\frac{\partial v_j(\boldsymbol{x})}{\partial \boldsymbol{x}_i}$  for  $i \in \mathcal{C}, j \in \mathcal{M}$ . Strategy 2): replace  $v_j(\cdot)$  by its real-time voltage measurement  $v_j^{\text{mea}}(t)$  for  $j \in \mathcal{M}$ .

To implement Strategy 1), we adopt the ES control method [10] and add a small sinusoidal probing signal to each power injection with

$$\hat{\boldsymbol{x}}_i(t) = \boldsymbol{x}_i(t) + a\sin(\boldsymbol{\omega}_i t), \quad i \in \mathcal{C}$$
 (7)

where a is the small amplitude<sup>1</sup> and the sinusoidal signal is

$$\sin(\boldsymbol{\omega}_i t) := \begin{cases} \sin(\omega_i t), & i \in \mathcal{C}_{\text{svc}} \\ [\sin(\omega_i^p t), \sin(\omega_i^q t)]^\top, & i \in \mathcal{C}_{\text{dg}}. \end{cases}$$
(8)

Let  $N = |\mathcal{C}_{\text{svc}}| + 2|\mathcal{C}_{\text{dg}}|$  be the dimensionality of the decision variable x. Define  $\sin(\omega t) := (\sin(\omega_i t))_{i \in \mathcal{C}} \in \mathbb{R}^N$  as the column vector that collects all the sinusoidal signals. The frequencies  $\omega := (\omega_i)_{i \in \mathcal{C}}$  are selected as

$$\omega_n = \frac{2\pi}{\varepsilon_\omega} \kappa_n, \quad \forall n \in [N] := \{1, \dots, N\}$$
 (9)

where  $\varepsilon_{\omega}$  is a small positive parameter and  $\kappa_i \neq \kappa_j$  for all  $i \neq j$  are rational numbers. In this way, each element  $x_n$  in x is assigned with a particular frequency  $\omega_n$ .

Based on the above description, the P-PDGD (5) is modified as the ES-P-PDGD (10):

$$\dot{\boldsymbol{x}}_{i} = k_{x} \Big[ \operatorname{Proj}_{\hat{\mathcal{X}}_{i}} \left( \boldsymbol{x}_{i} - \alpha_{x} \boldsymbol{h}_{i} (\boldsymbol{x}_{i}, \boldsymbol{\lambda}, \boldsymbol{\xi}_{i}^{j}) \right) - \boldsymbol{x}_{i} \Big], \quad i \in \mathcal{C} \quad (10a)$$

$$\dot{\lambda}_{j}^{+} = k_{\lambda} \Big[ \operatorname{Proj}_{\mathbb{R}_{+}} \left( \lambda_{j}^{+} + \alpha_{\lambda} (\mu_{j} - \bar{v}_{j}) \right) - \lambda_{j}^{+} \Big], \quad j \in \mathcal{M} \quad (10b)$$

$$\dot{\lambda}_{j}^{-} = k_{\lambda} \Big[ \operatorname{Proj}_{\mathbb{R}_{+}} \left( \lambda_{j}^{-} + \alpha_{\lambda} (\underline{v}_{j} - \mu_{j}) \right) - \lambda_{j}^{-} \Big], \quad j \in \mathcal{M} \quad (10c)$$

$$\dot{\boldsymbol{\xi}}_{i}^{j} = \frac{1}{\epsilon} \Big[ -\boldsymbol{\xi}_{i}^{j} + \frac{2}{a} v_{j} (\hat{\boldsymbol{x}}(t)) \sin(\boldsymbol{\omega}_{i} t) \Big], \quad j \in \mathcal{M}, i \in \mathcal{C} \quad (10d)$$

$$\dot{\mu}_{j} = \frac{1}{\epsilon} \Big[ -\mu_{j} + v_{j} (\hat{\boldsymbol{x}}(t)) \Big], \quad j \in \mathcal{M} \quad (10e)$$

<sup>&</sup>lt;sup>1</sup>For notational simplicity, we adopt an identical amplitude a for all power injections here. In practice, different amplitude parameters can be used.

where  $\epsilon$  is a small positive parameter, and

$$\hat{\boldsymbol{x}}(t) := \boldsymbol{x}(t) + a\sin(\omega t) \tag{11a}$$

$$\boldsymbol{h}_i(\boldsymbol{x}_i, \boldsymbol{\lambda}, \boldsymbol{\xi}_i^j) := \nabla c_i(\boldsymbol{x}_i) + \sum_{j \in \mathcal{M}} (\lambda_j^+ - \lambda_j^-) \boldsymbol{\xi}_i^j.$$
 (11b)

The key difference between P-PDGD (5) and ES-P-PDGD (10) is the introduction of new variables  $\boldsymbol{\xi} := (\boldsymbol{\xi}_i^j)_{j \in \mathcal{M}, i \in \mathcal{C}}$  and  $\boldsymbol{\mu} := (\mu_j)_{j \in \mathcal{M}}$ . We explain the rationale and benefits of this modification with Remark 3. To ensure the actual power injection  $\hat{\boldsymbol{x}}_i \in \mathcal{X}_i$ , we replace  $\mathcal{X}_i$  with the shrunken feasible set  $\hat{\mathcal{X}}_i$  in (10a). As  $a \to 0^+$ ,  $\hat{\mathcal{X}}$  recovers to  $\mathcal{X}$ .

$$\hat{\mathcal{X}_i}\!:=\!\begin{cases} \underline{q}_i\!+\!a\!\leq q_i \leq \bar{q}_i\!-\!a, & i\in\mathcal{C}_{\mathrm{svc}}\\ \underline{p}_i\!+\!a\!\leq p_i \leq \bar{p}_i\!-\!a, \; p_i^2\!+\!q_i^2\!\leq\!(\bar{s}_i\!-\!\sqrt{2}a)^2, \; i\!\in\mathcal{C}_{\mathrm{dg}}. \end{cases}$$

**Remark 3.** (Fast Dynamics of  $\boldsymbol{\xi}$  and  $\boldsymbol{\mu}$ .) In essence,  $\boldsymbol{\xi}_i^j$  and  $\mu_j$  are the real-time approximations of the gradient  $\frac{\partial v_j}{\partial \boldsymbol{x}_i}$  and the value  $v_j$ , respectively. The intuition behind is that by setting  $\epsilon$  sufficiently small, the dynamics of  $\boldsymbol{\xi}_i^j$  and  $\mu_j$ , i.e., (10d) (10e), operate in a faster time scale compared to the dynamics of  $(\boldsymbol{x}, \boldsymbol{\lambda})$ . The advantages of introducing these fast dynamics of  $\boldsymbol{\xi}$  and  $\boldsymbol{\mu}$  include:

- 1) It facilitates the analysis of the algorithm via averaging theory, since the time-variant sinusoidal signals do not appear inside the projection operators. Moreover, the fast dynamics are linear, which can be easily handled by singular perturbation theory.
- 2) The fast dynamics (10d) (10e) can be seen as low-pass filters, which can diminish the oscillations and improve the transient performance of the closed-loop system.

Since  $\hat{x}(t)$  is the actual power injection to the physical system at time t, we can substitute  $v_j(\hat{x})$  with the voltage measurement  $v_j^{\text{mea}}(t)$  in (10), i.e., Strategy 2). Consequently, we develop the model-free optimal voltage control (MF-OVC) algorithm as Algorithm 1, which is indeed the ES-P-PDGD (10) with the measurement substitution.

# Algorithm 1 Model-Free Optimal Voltage Control Alg.

At every time t, perform the following steps:

• Each monitored bus  $j \in \mathcal{M}$  measures the local voltage magnitude  $v_j^{\text{mea}}(t)$ , updates  $(\lambda_j^+, \lambda_j^-, \mu_j)$  according to

$$\dot{\mu}_j = \frac{1}{\epsilon} \left[ -\mu_j + v_j^{\text{mea}}(t) \right] \tag{12b}$$

and broadcasts  $(v_j^{\text{mea}}(t),\lambda_j^+(t),\lambda_j^-(t))$  to every controllable device  $i\in\mathcal{C}.$ 

• Each controllable device  $i \in \mathcal{C}$  updates  $(\boldsymbol{x}_i, \boldsymbol{\xi}_i^j)$  by

$$\dot{\boldsymbol{\xi}}_{i}^{j} = \frac{1}{\epsilon} \left[ -\boldsymbol{\xi}_{i}^{j} + \frac{2}{a} v_{j}^{\text{mea}}(t) \sin(\boldsymbol{\omega}_{i} t) \right], \ j \in \mathcal{M}$$
 (13b)

and executes power injection  $\hat{x}_i(t) = x_i(t) + a\sin(\omega_i t)$ .

The implementation of the proposed MF-OVC algorithm is illustrated in Figure 1. Each monitored bus  $j \in \mathcal{M}$  measures

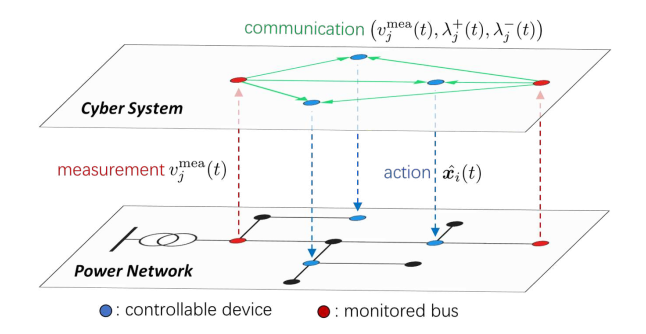


Fig. 1. Schematic of the proposed MF-OVC mechanism.

its local voltage magnitude  $v_j^{\text{mea}}$  from the physical layer, then updates  $(\mu_j, \lambda_j^+, \lambda_j^-)$  and communicates  $(v_j^{\text{mea}}, \lambda_j^+, \lambda_j^-)$  in the cyber layer. Each controllable device  $i \in \mathcal{C}$  updates  $(\boldsymbol{\xi}_i^j, \boldsymbol{x}_i)$  based on the received information, and the power injection command  $\hat{\boldsymbol{x}}_i$  is executed in the physical layer. Then the power network responses to the power injection  $\hat{\boldsymbol{x}}$  and presents the corresponding voltage profiles  $\boldsymbol{v}(\hat{\boldsymbol{x}})$ . This forms a closed-loop feedback control system. Although the MF-OVC algorithm is developed based on a static OVC problem (1), it can adapt fast to dynamical system environments and handle voltage violation under time-varying power disturbances, due to the feedback mechanism and exploitation of real-time measurements. As a result, the proposed algorithm unifies all the merits described in the introduction section.

## IV. PERFORMANCE ANALYSIS

This section presents the stability properties and the robustness to measurement noises of the MF-OVC algorithm.

## A. Stability Analysis of ES-P-PDGD

Denote  $z:=[x;\lambda]$  and  $\hat{\mathcal{X}}:=\prod_{i\in\mathcal{C}}\hat{\mathcal{X}}_i$ . Let  $\hat{Z}:=\hat{\mathcal{X}}\times\mathbb{R}^{2|\mathcal{M}|}_+$  be the feasible set of z in the ES-P-PDGD (10), and  $K:=(2|\mathcal{C}_{\mathrm{dg}}|+|\mathcal{C}_{\mathrm{svc}}|+1)|\mathcal{M}|$  be the dimensionality of  $[\xi;\mu]$ . Denote  $\hat{\mathcal{A}}$  as the saddle point set for the saddle point problem (4) with  $\hat{\mathcal{X}}$ , i.e., any point  $z^*\in\hat{\mathcal{A}}$  is an optimal solution of (4) with  $\hat{\mathcal{X}}$ . Denote the distance between z and  $\hat{\mathcal{A}}$  as

$$||z||_{\hat{\mathcal{A}}} := \inf_{oldsymbol{lpha} \in \hat{\mathcal{A}}} ||z-oldsymbol{lpha}||.$$

**Definition 1.** A continuous function  $\beta(r,t): \mathbb{R}_+ \times \mathbb{R}_+ \to \mathbb{R}_+$  is said to be of class- $\mathcal{KL}$  if it is zero at zero and strictly increasing in the first argument r, and non-increasing in the second argument t and converging to zero as  $t \to +\infty$ .

**Theorem 2.** (Semi-Global Practical Asymptotical Stability.) Suppose that the saddle point set  $\hat{A}$  is compact. Under Assumption 2 and 3, there exists a class- $\mathcal{KL}$  function  $\beta$  such that for any compact set  $\mathcal{D} \subset \hat{Z} \times \mathbb{R}^K$  of initial condition, any desired precision  $\nu > 0$ , there exists  $\epsilon^* > 0$  such that for any  $\epsilon \in (0, \epsilon^*)$ , there exists  $a^* > 0$  such that for any  $a \in (0, a^*)$ , there exists  $\varepsilon_{\omega}^* > 0$  such that for any  $\varepsilon_{\omega} \in (0, \varepsilon_{\omega}^*)$ , the trajectory  $\mathbf{z}(t)$  of the ES-P-PDGD (10) satisfies

$$||z(t)||_{\hat{\mathcal{A}}} \le \beta(||z(t_0)||_{\hat{\mathcal{A}}}, t - t_0) + \nu, \quad \forall t \ge t_0.$$
 (14)

The proof of Theorem 2 is provided in Appendix I.

Remark 4. We explain the key observations as below:

- Due to the small probing sinusoidal signals  $a\sin(\omega t)$  in the ES-P-PDGD (10), the state z will not converge to a fixed point anymore, but rather to a small  $\nu$ -neighborhood of  $\hat{\mathcal{A}}$ . This property is described by the bound (14). By setting the parameters  $(\epsilon, a, \varepsilon_{\omega})$  sufficiently small, one can make this precision  $\nu$  as small as desired.
- As  $(\epsilon, a, \varepsilon_{\omega}) \to 0^+$ , the ES-P-PDGD (10) recovers the same convergence rate of the P-PDGD (5), as indicated in the proof of Theorem 2.
- As stated in Theorem 2, the tuning order of parameters is relevant: first set  $\epsilon$  sufficiently small, then a, and lastly  $\epsilon_{\omega}$ . This order comes mainly from the proof and can guide us on how to tune these parameters in practice.

#### B. Robustness to Measurement Noise

The following corollary of Theorem 2 [9] indicates that this algorithm is robust to *small additive* measurement noise. Moreover, the numerical simulations in Section V-D verify the robustness even when the noise is relatively large.

**Corollary 1.** (Structural Robustness.) For any tuple of  $(\epsilon, a, \varepsilon_{\omega})$  that induces the bound (14), under the same conditions in Theorem 2, there exists  $\rho^* > 0$  such that for any measurement noise  $\mathbf{d} : \mathbb{R}_+ \to \mathbb{R}^{|\mathcal{M}|}$  with  $\sup_{t \geq t_0} ||\mathbf{d}(t)|| \leq \rho^*$ , the trajectory  $\mathbf{z}(t)$  of the ES-P-PDGD (10) with additive measurement noise  $\mathbf{d}$  satisfies

$$||z(t)||_{\hat{A}} \le \beta(||z(t_0)||_{\hat{A}}, t - t_0) + 2\nu, \quad \forall t \ge t_0.$$
 (15)

Comparing with (14), the ES-P-PDGD (10) with small additive measurement noise d maintains similar convergence results, and noise d leads to an additional  $\nu$  term in (15).

## V. NUMERICAL SIMULATIONS

## A. Simulation Setup

The modified PG&E 69-bus distribution system, shown as Figure 2, is used as the test system. There are three PV plants at bus 35, 54 and 69, which operate in the maximum power point tracking mode. The controllable devices include three SVCs (located at bus 35, 42 and 67) and three DGs (located at bus 20, 40, 50). We select bus 3, 27, 35, 50, 54 and 69 as the monitored buses. The voltage of bus 0 (slack bus) is  $10.5~\rm kV$  (1 p.u.), and the lower and upper bounds of voltage magnitude are set as 0.95 p.u. and 1.05 p.u., respectively. We use the quadratic cost function in objective (1a). For the MF-OVC algorithm, we set a=0.05,  $\epsilon=0.02$ ,  $\epsilon_\omega=0.05$ , and  $\kappa_n=2n-1$  for  $n=1,\cdots,9$ .

Although an affine system model v(x) is assumed for theoretical analysis, we perform all simulations based on a full nonconvex AC power flow model using Matpower [24].

#### B. Static Voltage Control Under Step Power Change

Consider the test scenario when the three PV plants are suddenly shut down at time t=0 and all loads remain fixed. Due to the curtailment of PV generation and heavy loads, the distribution system violates the lower voltage limit

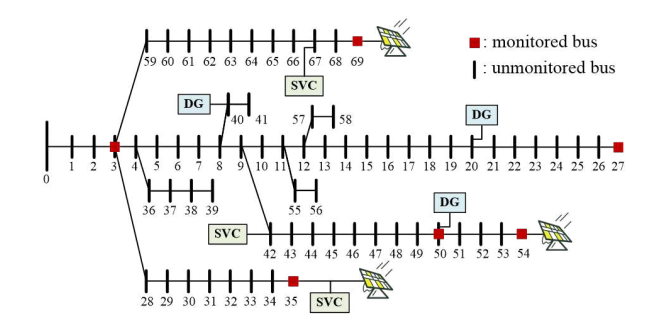


Fig. 2. The modified PG&E 69-bus distribution feeder.

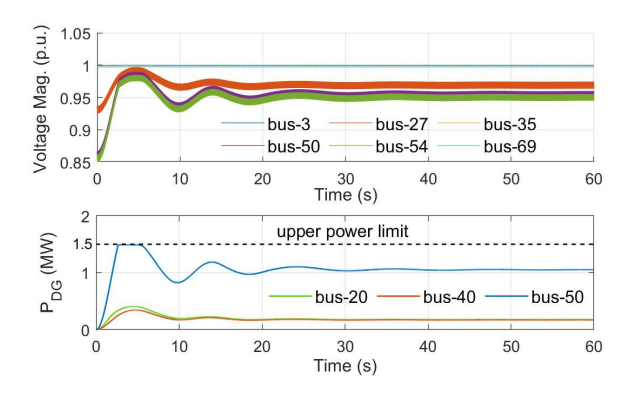


Fig. 3. Voltage dynamics of the monitored buses (upper plot) and active power outputs of DGs (lower plot) under step power change.

at many buses. We ran the proposed MF-OVC algorithm for voltage regulation from the start time t=0. The simulation results are shown as Figure 3. It is observed that the MF-OVC algorithm effectively brought the voltage magnitudes of monitored buses back to the acceptable range. The small high-frequency oscillations in voltage are caused by the probing sinusoidal signals. It is also seen that the DG power outputs converge to fixed values within tens of seconds, and the power capacity constraints are satisfied all the time. In addition, we solve the OVC model (1) with the linearized Distflow model [1] to obtain the optimal solution  $\boldsymbol{x}^*$ , which turns out to be the converged values of the MF-OVC algorithm and thus verifies its optimality.

#### C. Dynamic Voltage Control Under Continuous Change

To test the MF-OVC algorithm under time-varying disturbance, we add a 10% random perturbation to the loads, and a real-world PV generation profile is applied to the three PV plants in the test system. We ran the MF-OVC algorithm for voltage control and compared it with the case without voltage control. The simulation results are illustrated in Figure 4. Without voltage control, the test system frequently violates the lower or upper voltage limits as the PV generation fluctuates. In contrast, the proposed MF-OVC algorithm can adapt to the continuous power disturbances and maintain the voltage profiles within the acceptable range.

## D. Impact of Measurement Noise

To study the impact of measurement noises, we apply the noisy voltage measurement  $\tilde{v}_{j}^{\text{mea}}(t)$ , whose deviation from

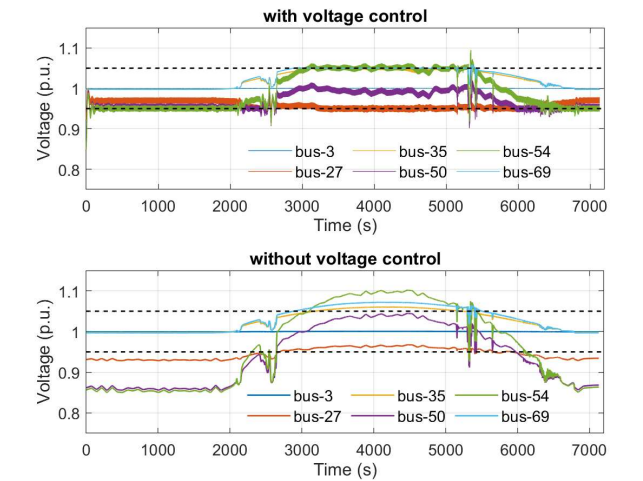


Fig. 4. Voltage dynamics of monitored buses under continuous disturbances (black dashed lines: upper (1.05 p.u.) and lower (0.95 p.u.) voltage limits).

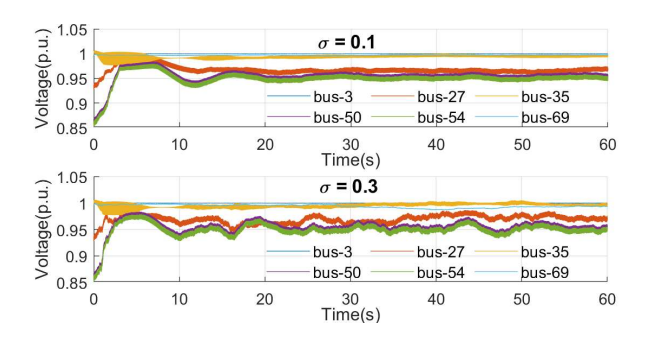


Fig. 5. Voltage dynamics of monitored buses with noisy measurements.

the base voltage value (1 p.u.) follows (16):

$$\tilde{v}_i^{\text{mea}}(t) - 1 = (v_i(\boldsymbol{x}(t)) - 1) \times (1 + \delta_i(t)),$$
 (16)

where  $v_j(\boldsymbol{x}(t))$  denotes the true voltage magnitude, and  $\delta_j$  is the perturbation ratio. We assume that  $\delta_j$  is a Gaussian random variable with  $\delta_j \sim \mathcal{N}(0,\sigma^2)$ , which is independent across time t and other monitored buses. We tune the standard deviation  $\sigma$  from 0.1 to 0.3 to simulate different levels of noises and test the performance of the MF-OVC algorithm under step power changes. The simulation results are shown as Figure 5, and the noiseless case with  $\sigma=0$  is illustrated as Figure 3. As expected, larger noise amplitudes lead to higher oscillations in the voltage dynamics. While the MF-OVC algorithm is robust to the voltage measurement noises and can restore the voltage profiles in all the cases.

#### VI. CONCLUSION

In this paper, we developed a real-time model-free optimal voltage control algorithm based on projected primal-dual gradient dynamics and ES control. The proposed algorithm operates purely based on the voltage measurement and does not require any other network information. With appropriate parameters, this algorithm can effectively bring the monitored voltage magnitudes back to the acceptable range with minimum operational cost, while respecting the power

capacity constraints all the time. Numerical simulations on the PG&E 69-bus distribution feeder demonstrated the optimality, adaptivity, and robustness of the proposed algorithm.

## APPENDIX I PROOF OF THEOREM 2

Denote  $s_1 := [x; \lambda]$ ,  $s_2 := [\xi; \mu]$ , and  $s := [s_1; s_2]$ . The ES-P-PDGD (10) is reformulated in compact form as

$$\dot{\boldsymbol{s}} = \begin{bmatrix} \dot{\boldsymbol{s}}_1 \\ \dot{\boldsymbol{s}}_2 \end{bmatrix} = \begin{bmatrix} \boldsymbol{g}_1(\boldsymbol{s}_1, \boldsymbol{s}_2) \\ \frac{1}{\epsilon}(-\boldsymbol{s}_2 + \boldsymbol{g}_2(t, \boldsymbol{s}_1)) \end{bmatrix} := \boldsymbol{g}(t, \boldsymbol{s}), \quad (17)$$

where the function  $g_1(s_1, s_2)$  captures the dynamics (10a)-(10c), and function  $g_2(t, s_1)$  is given by

$$\mathbf{g}_{2} := \begin{bmatrix} \left(\frac{2}{a}v_{j}(\mathbf{x} + a\sin(\boldsymbol{\omega}t))\sin(\omega_{n}t)\right)_{n \in [N], j \in \mathcal{M}} \\ \left(v_{j}(\mathbf{x} + a\sin(\boldsymbol{\omega}t))\right)_{j \in \mathcal{M}} \end{bmatrix}, \quad (18)$$

which associates with dynamics (10d) of  $\xi$  and (10e) of  $\mu$ .

The following Lemma 1 characterizes the average map for the function  $g_2(t, s_1)$ . Lemma 1 can be proved by considering the multivariate Taylor expansion of  $g_2(t, s_1)$  and using [9, Lemma 7.1].

**Lemma 1.** The average of function  $g_2(t, s_1)$  is given by

$$g_2^{av}(s_1) := \frac{1}{T} \int_0^T g_2(t, s_1) dt = \ell(s_1) + \mathcal{O}(a),$$
 (19)

where 
$$\ell(s_1) := \begin{bmatrix} (\frac{\partial v_j(x)}{\partial x_n})_{n \in [N], j \in \mathcal{M}} \\ (v_j(x))_{j \in \mathcal{M}} \end{bmatrix}$$
, and  $T$  is the minimum common period of the sinusoidal signals  $\sin(\omega t)$ .

We analyze the stability properties of system (17) via averaging theory and singular perturbation theory as follows. **Step 1**) *Construct a compact set for analysis.* 

To apply general averaging theory and singular perturbation theory, it usually requires that the considered trajectories stay within predefined compact sets. Without loss of generality, we consider the compact set  $[(\hat{\mathcal{A}} + \Delta \mathbb{B}) \cap \hat{\mathcal{Z}}] \times \Delta \mathbb{B}$  for the initial condition  $s(t_0)$  and any desired  $\Delta > 0$ . Here,  $\mathbb{B}$  denotes a closed unit ball of appropriate dimension, and  $\hat{\mathcal{A}} + \Delta \mathbb{B}$  denotes the union of all sets obtained by taking a closed ball of radius  $\Delta$  around each point in the saddle point set  $\hat{\mathcal{A}}$ . By Theorem 1, there exists a class- $\mathcal{KL}$  function  $\beta$  such that for any initial condition  $z(t_0) \in \hat{\mathcal{Z}}$ , the trajectory z(t) of the P-PDGD (5) with the feasible set  $\hat{\mathcal{X}}$  satisfies

$$||z(t)||_{\hat{A}} \le \beta(||z(t_0)||_{\hat{A}}, t - t_0), \quad \forall t \ge t_0.$$
 (20)

Without loss of generality, we assume the desired convergence precision  $\nu \in (0,1)$ . Using the  $\beta$  function in (20), we define the set

$$\mathcal{F} := \left\{ \boldsymbol{s}_1 \in \hat{\mathcal{Z}} : ||\boldsymbol{s}_1||_{\hat{\mathcal{A}}} \le \beta \left( \max_{\boldsymbol{p} \in \hat{\mathcal{A}} + \Delta \mathbb{B}} ||\boldsymbol{p}||_{\hat{\mathcal{A}}}, 0 \right) + 1 \right\}, (21)$$

which is compact. Due to the boundedness of  $\mathcal{F}$ , there exists a positive constant  $M_1$  such that  $\mathcal{F} \subset M_1\mathbb{B}$ . Since  $\ell(s_1)$  (defined in Lemma 1) is continuous by Assumption 2, there exists a positive constant  $M_2 > \Delta$  such that  $||\ell(s_1)|| + 1 \leq M_2$  whenever  $||s_1|| \leq M_1$ . We then study the behavior of system (17) restricted to evolve in the compact set  $\mathcal{F} \times M_2\mathbb{B}$ .

**Step 2)** Study the stability of the average system.

By definition (9), the sinusoidal signals in system (17) are given by  $\sin(\frac{2\pi}{\varepsilon_{\omega}}\kappa_n t)$  for  $n \in [N]$ . For sufficiently small  $\varepsilon_{\omega}$ , system (17), evolving in  $\mathcal{F} \times M_2\mathbb{B}$ , is in standard form for the application of averaging theory [25]. By Lemma 1, we derive the autonomous **average system** of system (17):

$$\begin{bmatrix} \dot{\boldsymbol{y}}_1 \\ \dot{\boldsymbol{y}}_2 \end{bmatrix} = \frac{1}{T} \int_0^T \boldsymbol{g}(t, \boldsymbol{y}) dt = \begin{bmatrix} \boldsymbol{g}_1(\boldsymbol{y}_1, \boldsymbol{y}_2) \\ \frac{1}{\epsilon}(-\boldsymbol{y}_2 + \boldsymbol{\ell}(\boldsymbol{y}_1) + \mathcal{O}(a)) \end{bmatrix}, (22)$$

where  $y := [y_1; y_2]$  takes the same form as  $s := [s_1; s_2]$ .

To analyze the average system (22), we can first ignore the small  $\mathcal{O}(a)$ -perturbation by setting a=0. Thus the resultant system is in the standard form for the application of singular perturbation theory. As  $\epsilon \to 0^+$ , we freeze the slow state  $y_1$ , then the **boundary layer system** of the average system (22) with a=0 in the time scale  $\tau=t/\epsilon$  is given by  $\frac{dy_2}{d\tau}=-y_2+\ell(y_1)$ , which is a linear system with unique equilibrium point  $y_2^*=\ell(y_1)$ . Thus the **reduced system** is

$$\dot{\boldsymbol{y}}_1 = \boldsymbol{g}_1(\boldsymbol{y}_1, \boldsymbol{\ell}(\boldsymbol{y}_1)), \tag{23}$$

which is precisely the P-PDGD (5). By Theorem 1 and [25, Theorem 1], it follows that as  $\epsilon \to 0^+$ , the set  $\hat{\mathcal{A}} \times M_2\mathbb{B}$  is semi-globally practically asymptotically stable (**SGPAS**) for system (22) with a=0. Then by the structural robustness results for continuous ordinary differential equations [9, Proposition A.1], the set  $\hat{\mathcal{A}} \times M_2\mathbb{B}$  is also SGPAS for the average system (22) as  $(\epsilon, a) \to 0^+$ , i.e., Lemma 2.

**Lemma 2.** Given the precision  $\nu$ , there exists  $\epsilon^* > 0$  such that for any  $\epsilon \in (0, \epsilon^*)$ , there exists  $a^* > 0$  such that for any  $a \in (0, a^*)$ , with initial condition  $\mathbf{y}(t_0) \in [(\hat{A} + \Delta \mathbb{B}) \cap \hat{\mathcal{Z}}] \times \Delta \mathbb{B}$ , the solution  $\mathbf{y}(t)$  of the average system (22) satisfies

$$||\mathbf{y}_1(t)||_{\hat{\mathcal{A}}} \le \beta(||\mathbf{y}_1(t_0)||_{\hat{\mathcal{A}}}, t - t_0) + \frac{\nu}{2}, \ \forall t \ge t_0.$$
 (24)

The completeness of solution y(t) for system (22) follows [26, Lemma 5] and the structure of the set  $\mathcal{F}$  (21). See [23] for a detailed proof.

**Step 3)** Link average system (22) to original system (17).

Since the set  $\hat{\mathcal{A}} \times M_2\mathbb{B}$  is SGPAS for the average system (22) as  $(\epsilon, a) \to 0^+$ , by averaging theory for perturbed systems [9, Theorem 7], we directly obtain that for each pair of  $(\epsilon, a)$  inducing the bound (24), there exists  $\varepsilon_{\omega}^* > 0$  such that for any  $\varepsilon_{\omega} \in (0, \varepsilon_{\omega}^*)$ , the solution s(t) of the original system (17) restricted to  $\mathcal{F} \times M_2\mathbb{B}$  satisfies

$$||s_1(t)||_{\hat{A}} \le \beta(||s_1(t_0)||_{\hat{A}}, t - t_0) + \nu, \quad \forall t \ge t_0.$$
 (25)

The completeness of solution s for system (17) is guaranteed by the construction of  $M_2$ . Thus Theorem 2 is proved.

#### REFERENCES

- [1] G. Qu and N. Li, "Optimal distributed feedback voltage control under limited reactive power," *IEEE Trans. Power Syst.*, vol. 35, no. 1, pp. 315–331, 2020.
- [2] H. Zhu and H. J. Liu, "Fast local voltage control under limited reactive power: Optimality and stability analysis," *IEEE Trans. Power Syst.*, vol. 31, no. 5, pp. 3794–3803, 2016.
- [3] J. Zhang, Z. Chen, C. He, Z. Jiang, and L. Guan, "Data-driven-based optimization for power system var-voltage sequential control," *IEEE Trans. Ind. Informat.*, vol. 15, no. 4, pp. 2136–2145, 2019.

- [4] H. Zhang, J. Zhou, Q. Sun, J. M. Guerrero, and D. Ma, "Data-driven control for interlinked ac/dc microgrids via model-free adaptive control and dual-droop control," *IEEE Trans. Smart Grid*, vol. 8, no. 2, pp. 557–571, 2017.
- [5] H. Xu, A. D. Domínguez-García, V. V. Veeravalli, and P. W. Sauer, "Data-driven voltage regulation in radial power distribution systems," *IEEE Trans. Power Syst.*, vol. 35, no. 3, pp. 2133–2143, 2020.
- [6] W. Wang, N. Yu, Y. Gao, and J. Shi, "Safe off-policy deep reinforcement learning algorithm for volt-var control in power distribution systems," *IEEE Trans. Smart Grid*, vol. 11, no. 4, pp. 3008–3018, 2020.
- [7] Y. Zhang, X. Wang, J. Wang, and Y. Zhang, "Deep reinforcement learning based volt-var optimization in smart distribution systems," *IEEE Trans. Smart Grid*, vol. 12, no. 1, pp. 361–371, 2021.
- [8] X. Chen, G. Qu, Y. Tang, S. Low, and N. Li, "Reinforcement learning for decision-making and control in power systems: Tutorial, review, and vision," arXiv preprint arXiv:2102.01168, 2021.
- [9] J. I. Poveda and N. Li, "Robust hybrid zero-order optimization algorithms with acceleration via averaging in time," *Automatica*, vol. 123, p. 109361, 2021.
- [10] K. B. Ariyur and M. Krstić, Real Time Optimization by Extremum Seeking Control. Wiley Online Library, 2003.
- [11] J. I. Poveda and A. R. Teel, "A framework for a class of hybrid extremum seeking controllers with dynamic inclusions," *Automatica*, no. 76, pp. 113–126, 2017.
- [12] M. Ye and G. Hu, "Distributed extremum seeking for constrained networked optimization and its application to energy consumption control in smart grid," *IEEE Trans. Control Syst. Technol.*, vol. 24, no. 6, pp. 2048–2058, 2016.
- [13] M. D. Sankur, R. Dobbe, A. von Meier, and D. B. Arnold, "Model-free optimal voltage phasor regulation in unbalanced distribution systems," *IEEE Trans. Smart Grid*, vol. 11, no. 1, pp. 884–894, 2020.
- [14] X. Li, Y. Li, and J. E. Seem, "Maximum power point tracking for photovoltaic system using adaptive extremum seeking control," *IEEE Trans. Control Syst. Technol.*, vol. 21, no. 6, pp. 2315–2322, 2013.
- [15] D. B. Arnold, M. Negrete-Pincetic, M. D. Sankur, D. M. Auslander, and D. S. Callaway, "Model-free optimal control of var resources in distribution systems: An extremum seeking approach," *IEEE Trans. Power Syst.*, vol. 31, no. 5, pp. 3583–3593, 2016.
- [16] H. Nazaripouya, H. R. Pota, C. Chu, and R. Gadh, "Real-time model-free coordination of active and reactive powers of distributed energy resources to improve voltage regulation in distribution systems," *IEEE Trans. Sustain. Energy*, vol. 11, no. 3, pp. 1483–1494, 2020.
- [17] J. Johnson, A. Summers, R. Darbali-Zamora, J. Hernandez-Alvidrez, J. Quiroz, D. Arnold, and J. Anandan, "Distribution voltage regulation using extremum seeking control with power hardware-in-the-loop," *IEEE J. Photovolt.*, vol. 8, no. 6, pp. 1824–1832, 2018.
- [18] Y. Chen, A. Bernstein, A. Devraj, and S. Meyn, "Model-free primal-dual methods for network optimization with application to real-time optimal power flow," in 2020 American Control Conference (ACC), 2020, pp. 3140–3147.
- [19] X.-B. Gao, "Exponential stability of globally projected dynamic systems," *IEEE Trans. Neural Netw.*, vol. 14, no. 2, pp. 426–431, 2003.
- [20] A. Nagurney and D. Zhang, Projected Dynamical Systems and Variational Inequalities with Applications. Springer Science & Business Media, 2012, vol. 2.
- [21] Y. Zhu, W. Yu, G. Wen, and G. Chen, "Projected primal-dual dynamics for distributed constrained nonsmooth convex optimization," *IEEE Trans. Cybern.*, vol. 50, no. 4, pp. 1776–1782, 2020.
- [22] P. Bansode, V. Chinde, S. Wagh, R. Pasumarthy, and N. Singh, "On the exponential stability of projected primal-dual dynamics on a riemannian manifold," arXiv preprint arXiv:1905.04521, 2019.
- [23] X. Chen, J. I. Poveda, and N. Li, "Model-free optimal voltage control via continuous-time zeroth-order methods," arXiv preprint arXiv:2103.14703, 2021.
- [24] R. D. Zimmerman, C. E. Murillo-Sánchez, and R. J. Thomas, "Matpower: Steady-state operations, planning and analysis tools for power systems research and education," *IEEE Trans. Power Syst.*, vol. 26, no. 1, pp. 12–19, Feb. 2011.
- [25] A. R. Teel, L. Moreau, and D. Nesic, "A unified framework for input-to-state stability in systems with two time scales," *IEEE Trans. Autom. Control*, vol. 48, no. 9, pp. 1526–1544, 2003.
- [26] S. Park, N. Martins, and J. Shamma, "Payoff dynamics model and evolutionary dynamics model: Feedback and convergence to equilibria," arXiv:1903.02018v4, 2020.